



Drivers of long-term changes in summer compound hot extremes in China: Climate change, urbanization, and vegetation greening

Peng Ji ^{a,b}, Xing Yuan ^{a,b,c,*}, Feng Ma ^{a,b}, Qibo Xu ^d

^a Key Laboratory of Hydrometeorological Disaster Mechanism and Warning of Ministry of Water Resources/Collaborative Innovation Center on Forecast and Evaluation of Meteorological Disasters, Nanjing University of Information Science and Technology, Nanjing 210044, Jiangsu, China

^b School of Hydrology and Water Resources, Nanjing University of Information Science and Technology, Nanjing 210044, Jiangsu, China

^c Institute of Atmospheric Physics, Chinese Academy of Sciences, Beijing 100029, China

^d California NanoSystems Institute, University of California, Los Angeles (UCLA), Los Angeles, CA 90095, USA



ARTICLE INFO

Keywords:

Compound hot extremes
Climate change
Urbanization
3-D Building morphology
Vegetation greening
Attribution

ABSTRACT

Induced by numerous environmental and anthropogenic factors, the frequency of compound hot extremes (CoHot) is increasing globally. However, there is a lack of a comprehensive understanding of the relative importance of different factors in the change of CoHot, as most studies focused solely on individual factors. We systematically attribute the long-term trends of summertime CoHot in China to 24 factors including climate background, climate change, urbanization (including impervious area expansion and three-dimensional urban morphology), and vegetation change, using partial least square regression (PLSR) and variable importance projections for analysis. Cross-evaluation results based on 2259 meteorological stations indicate that the PLSR model accurately simulates the trends of CoHot frequency, duration, and intensity, with a relative error of 4–20% from national to individual station scales. A warm and humid climate background, rising average summertime temperatures, impervious area expansions, high building volume densities, low building heights, and vegetation wilting are the main factors that favoring the increasing and intensifying trends of CoHot. Although summertime warming contributes the most, the significance of urbanization and vegetation greening has been growing in recent years. Urbanization's contribution increases from 9.3% on a national scale to over 40% in urban centers, mainly due to increased building volume density rather than expansions of impervious area. In northern China, vegetation greening has reduced the local increasing trends in frequency/duration of CoHot by 20% to 40%, and such mitigation effects are primarily induced by increased vegetation cover. Our results suggest that, reducing building volume density and promoting vegetation greening can mitigate the increasing risk of CoHot under global warming.

1. Introduction

Extreme hot temperature events have devastating impacts on ecosystem, human health, and economy (Easterling et al., 2000; Li et al., 2021). Under the background of global warming, the significant increase in extreme hot temperature events globally is now indisputable (IPCC, 2021; Meehl and Tebaldi, 2004). Traditional hot extremes are defined based solely on the maximum daytime or minimum nighttime temperatures, also known as hot days or hot nights (Chen and Zhai, 2017). However, as global temperatures of daytime and nighttime continue to rise, the frequency of a type of persistent day-night combined heat event, called the compound hot extreme (CoHot), has been increasing over recent decades (Chen and Zhai, 2017; Ma and Yuan, 2021; Wang et al.,

2020a). Compared to solely daytime/nighttime heat, CoHots have a greater impact on human health, production safety, and social economics (Grimmond, 2007; Karl and Knight, 1997; Wang et al., 2021) and show larger increasing trends (Wu et al., 2023a). Climate model projections indicate that the occurrence and intensity of CoHot events will continue to increase in the future, especially under high-emission scenarios (Wang et al., 2020b; Xie et al., 2022; Yu et al., 2023). Therefore, understanding the drivers of CoHot changes is critical and urgent for developing mitigation measures and sustainable development policies.

Similar to independent hot days or nights, CoHot is influenced by numerous factors, including anthropogenic warming, urbanization, vegetation changes and climate background (Liao et al., 2021; Ma and

* Corresponding author at: Institute of Atmospheric Physics, Chinese Academy of Sciences, Beijing 100029, China.

E-mail address: xyuan2@mail.iap.ac.cn (X. Yuan).

Yuan, 2021; Wang et al., 2020a, 2021; Xu et al., 2022; Zhao et al., 2014). Massive emissions of anthropogenic greenhouse gases since the first Industrial Revolution have caused global warming and directly increased the risks associated with CoHot (Li et al., 2023; Wang et al., 2020a; Wang et al., 2022). The urbanization process modulates the hydrological, thermal and aerodynamic properties of land surface, resulting in higher temperatures in urban areas (also known as the urban heat island) (Carlson and Boland, 1978; Li et al., 2019; Taha, 1997; Wang and Li, 2021; Zhao et al., 2014). Some studies indicate that urbanization generally contributes positively to the increasing trend of CoHot frequency and intensity (Lin et al., 2024; Ma and Yuan, 2021; Wang et al., 2021). However, the extent of this contribution varies greatly across different studies (from <10% to over 50%), which is not only due to different local climate backgrounds, speeds of urbanization, and city sizes (Lin et al., 2024; Yang et al., 2022), but also related to the spatial scales of interest (Chao et al., 2020). In recent years, the impacts of climate background factors such as humidity and wind, and changes in vegetation, have also been increasingly explored (Yu et al., 2020; Zhao et al., 2014, 2023). However, most studies either focused on the effects of one or two factors or are limited to small regions, which makes it difficult to fully reveal the relative importance of various climate, environmental, and urbanization-related factors.

On the other hand, it should be noted that urbanization includes many processes, such as impervious area expansion and building construction, which influence urban temperatures in various approaches (Grimmond, 2007; Li et al., 2019). According to the traditional paradigm, the expansion of impervious areas weakens evapotranspiration cooling and results in higher temperatures in urban areas (Carlson and Boland, 1978; Taha, 1997), which may increase the frequency of hot extremes in cities. Recent studies, however, have highlighted the critical role of building height (which affects aerodynamic resistance) in the spatial variability of the urban heat island (Wang and Li, 2021; Zhao et al., 2014). Moreover, three-dimensional (3-D) building morphology, such as building height and building volume density, is highly correlated with warm nights (Paschalidis et al., 2021; Sobstyl et al., 2018) and high temperature in urban areas (Li et al., 2023; Shao et al., 2023). For example, Li et al. (2020a) directly simulated the urban climate of various cities with different volume density and morphology, and emphasized the significant role of urban volume density in sharpening urban heat island intensity. However, Shao et al. (2023) used machine learning algorithms to differentiate drivers of urban heat island, and found that the building height is more crucial. Therefore, the dominant factors contributing to urbanization's impact on high temperatures are still under debate. Additionally, most studies considering different urbanization factors focused on the urban heat island, leaving it unclear which primary urbanization process influence the changes of CoHot.

To address the research gaps mentioned above, this study proposes an attribution framework that can quantify the influences of numerous environmental factors related to climate change, climate background, urbanization, and vegetation changes on the long-term changes of CoHot. This framework is based on the partial least square regression model and variable importance projection (VIP) scores. The method has been applied in China to comprehensively investigate the dominant factors that have significantly influenced CoHot changes over recent decades, and to quantify their contributions from a national to a grid (1-km) scale. In addition, the contributions of different urbanization factors, such as building height, building volume density, and impervious area changes, to the overall impact of urbanization have also been compared.

2. Material and methods

2.1. Material

Daily maximum (T2Max) and minimum (T2Min) temperature observations from China Meteorological Administration (CMA)

meteorological stations during the summers from 1971 to 2017 were used to calculate the CoHot events. Following Ma and Yuan (2021), summers with 5 or more consecutive days of unobserved data were treated as missing seasons and stations with 5 or more missing summers were excluded. After this process, 2259 stations remained.

The 30-m annual maps of global artificial impervious area (GAIA) during 1985–2018 (Gong et al., 2020) were used to calculate the urban fraction (UrbF). Following previous research (Ma and Yuan, 2021), the UrbF values during 1979–1984 were set to the value of 1985 due to the lack of data. The 1-km maps of urban building height and building volume density were obtained from the three-dimensional (3D) building dataset developed based on the Synthetic Aperture Radar (SAR) (Li et al., 2020b). For each station, UrbF was defined as the proportion of impervious area within its buffer zone (e.g., a radius of 1 km), while building height (UrbH) and building volume density (UrbV) were directly obtained from the 1-km grids that contains the stations.

Monthly gridded meteorological forcings, including near-surface wind speed (U), surface downward shortwave radiation (SW), near-surface dew point temperature (Td), and total precipitation (P), were provided by the 5th generation of European ReAnalysis (ERA5) with a spatial resolution of 0.25° (Hersbach et al., 2020). Additionally, gridded T2Max and T2Min data from the 4-km TerraClimate dataset were utilized (Abatzoglou et al., 2018). The Global Land Surface Satellite (GLASS) dataset provided monthly data of leaf area index (LAI), fraction of vegetation cover (FVC), white-sky albedo (SKA) and black-sky albedo (BSA) at a spatial resolution of 0.05° (Liang et al., 2021). Meteorological forcings and GLASS products were remapped to station locations using the bilinear and nearest-neighbor interpolation methods, respectively.

2.2. Methods

Fig. 1 depicts the schematic diagram illustrating the definition and identification of CoHot events, along with the attribution approaches. Further details are provided below.

2.2.1. Definition and identification of compound hot extremes

According to previous studies (Ma and Yuan, 2021; Wang et al., 2020b), hot daytime (or nighttime) extreme events are defined as at least three consecutive days with T2Max (or T2Min) exceeds its 90th percentile. To avoid the attenuation of the annual cycle of thresholds and the inhomogeneity of percentile-based indices of extremes (Zhang et al., 2005), daily 90th percentile of T2Max (or T2Min) is derived from a 15-days window centered on a specific date during the baseline period (1971–2000). Thus, the number of samples used to estimate the 90th percentile threshold for a specific date is 450 (15 days × 30 years). CoHot events are defined as periods of at least three consecutive days with both hot daytime and nighttime extremes. The bottom left of **Fig. 1** shows a CoHot event at a station located at (50.25°N, 120.18°E) during July 9th–11th in 2002.

All summertime CoHot events during the summer days (May–September) of each year from 1971 to 2017 were identified. Run theory, which is widely used to identify drought/heatwave characteristics (Wang et al., 2021; Wang et al., 2020a), was then used to calculate the frequency, duration, and intensity of CoHot events for each year. Specifically, frequency and duration represent the count and total duration of CoHot events per year, respectively. Intensity is the average daily $\delta T2Max + \delta T2Min$ during CoHot events, where $\delta T2Max$ (or $\delta T2Min$) indicates the temperature departure from its 90th percentile on each day.

Linear trends of CoHot frequency, duration, and intensity for each station during 1971–2017 were calculated. The Getis-ord Gi* score (Getis and Ord, 1992), a regional clustering method, was used to identify hotspots and coldspots of CoHot variation. Hotspots (coldspots) indicate the linear trends of CoHot characteristics at the station and its surrounding areas are significantly larger (smaller) than the national average (Yang et al., 2022).

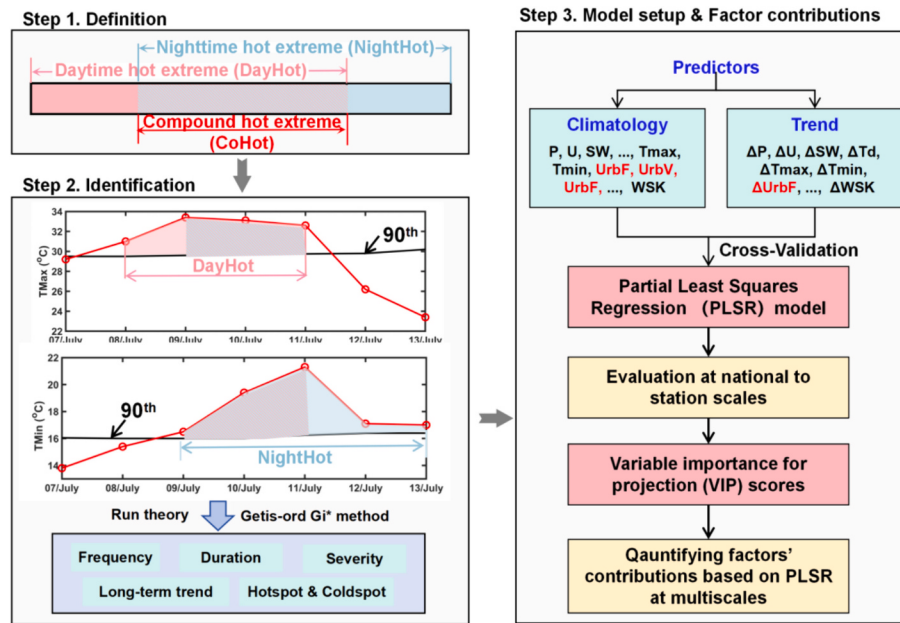


Fig. 1. Schematic diagram for quantifying the contributions of urbanization to the changes of compound hot extremes (CoHots) characteristics. Detailed information of predictors is presented in [Table 1](#).

2.2.2. Partial least square regression and variable importance for projection

Partial Least Square Regression (PLSR) models attempt to find multidimensional directions of predictors in X-space that explain the maximum variance of multidimensional directions of predictands in Y-space. Based on the PLSR model (the right panel of Fig. 1), the linear trend of CoHot characteristics (e.g., frequency, duration, or intensity), denoted as Y , are regressed onto different environmental and urbanization-related predictors x_i . The regression PLSR model can be represented as:

$$Y = a + \sum_{i=1}^N c f_i \times x_i \quad (1)$$

where a is the intercept, $c f_i$ is the regression coefficient for the i^{th} predictor x_i and N is the total number of predictors. The PLSR model takes

advantage of principle component analysis (PCA), classical correlation analysis (CCA), and multivariate linear regression (MLR) in solving the above regression model, so as to account for the multicollinearity when predictors are not independent of each other ([Hair et al., 2019](#); [Wu et al., 2023b](#)). It was constructed by extracting the latent factors of predictors and predictand with the aim of maximizing the covariance. Specifically, the first principle component (PC) was derived from all predictors based on the covariance matrix of predictors and predictand, and then regressed to the predictand. Multiple PCs were then continuously extracted from the remaining residuals of the predictors and regressed to the predictand until the threshold (e.g., the prescribed PC number) was reached. The increase in the total explained variance of the regression result in this study is $<1\%$ when the PC numbers are >10 (not shown), so the PC number was set at 10 to avoid overfitting. Note that the PCs are

Table 1
List of predictor variables.

No.	Variable name	Abbreviation	Units	Description	Source
1	Wind speed	U	m/s		ERA5
2	Downward shortwave radiation	SW	W/m ²		ERA5
3	Dew point temperature	Td	°C		ERA5
4	Precipitation	P	mm	Climatology during summer time of 1971–1990	ERA5
5	Maximum temperature	TMax	°C		Station/TerreClimate
6	Minimum temperature	TMin	°C		Station/TerreClimate
7	Urban fraction	UrbF	%		GAIA
8	Building height	UrbH	m		
9	Building volume density	UrbV	m ³ /km ²	Timely invariant	3D building
10	Leaf area index	LAI	m ² /m ²		GLASS AVHRR V50
11	Fraction of vegetation cover	FVC	%		GLASS AVHRR V40
12	White-sky albedo	WSA	—	Climatology during summer time of 1982–1990	GLASS MIX V50
13	Black-sky albedo	BSA	—		GLASS MIX V50
14	Trend of U	ΔU	m/s/decade		ERA5
15	Trend of SW	ΔSW	W/m ² /decade		ERA5
16	Trend of Td	ΔTd	°C/decade		ERA5
17	Trend of P	ΔP	mm/decade	Linear trend during 1971–2017	ERA5
18	Trend of TMax	ΔTMax	°C/decade		Station/TerreClimate
19	Trend of TMin	ΔTMin	°C/decade		Station/TerreClimate
20	Trend of UrbF	ΔUrbF	%/decade		GAIA
21	Trend of LAI	ΔLAI	m ² /m ² /decade		GLASS AVHRR V50
22	Trend of FVC	ΔFVC	%/decade		GLASS AVHRR V40
23	Trend of WSK	ΔWSA	—/decade	Linear trend during 1982–2017	GLASS MIX V50
24	Trend of BSK	ΔBSA	—/decade		GLASS MIX V50

linear combinations of the original predictors and are independent of each other. A more detailed description of the PLSR can be found in a previous study (Hair et al., 2019).

Predictors include climate backgrounds, long-term changes of meteorological forcings (e.g., P, Td, U, SW, TMax, and TMin), vegetation-related variables (e.g., LAI and FVC), urban features (e.g., UrbF, UrbH, and UrbV), and surface albedos (e.g., BSA and WSA). Climate backgrounds influence the sensitive of CoHot to the climate change and urbanization, thus modulating the spatial heterogeneity of CoHot changes. Detailed information is listed in Table 1, and all predictors were normalized before regression. Cross-validation was used to evaluate the modeling accuracy of the PLSR model, where 90% of randomly selected data from a total of 2261 stations were used for model construction, and the remaining 10% data were used for evaluation. The modeling accuracy (α) was quantified by using the ratio of simulated values (Y_o) to observed (Y) values as

$$\alpha = (Y_o / Y) \times 100\% \quad (2)$$

Variable Importance for Projection (VIP) scores are an efficient method for quantifying the importance of different predictors in the PLSR model (Farrés et al., 2015; Mahieu et al., 2023). Higher VIP values indicate higher importance, and predictors are typically considered significantly important when their VIP scores exceed 1 (Mahieu et al., 2023; Wu et al., 2023a). The principle of this index (Wold et al., 1993) is written as follows:

$$VIP_i = \sqrt{\frac{\sum_{f=1}^F \omega_{if}^2 \cdot SSY_f \cdot N}{SSY_{total} \cdot F}} \quad (3)$$

where VIP_i is the VIP score of the i^{th} predictors, ω_{if} represents the weight value between the i^{th} predictors and f^{th} PC component, and SSY_f denotes the sum of squares of the explained variance of the f^{th} PC component. SSY_{total} represents the total explained sum of squares of N predictors

(here is 24), and F denotes the total number of PC components (here is 10). The ω_{if} , SSY_f , and SSY_{total} are intermediate variables in the solution of Eq. (1). A more detailed description of the calculation of VIP can be found in previous study (Farrés et al., 2015; Mahieu et al., 2023).

2.2.3. Contributions of different factors

The contribution of a specific predictor (CT_i) is quantified through the following equation:

$$CT_i = \frac{Y_o - Y_{o,i}}{Y_o} \times 100\%$$

where $Y_{o,i}$ means setting the x_i to be 0 (for UrbH, UrbV, UrbF and all the long-term trend-related predictors) or the national mean value (for the climate background-related predictors) in the PLSR model. The contribution of urbanization (CT_{urb}) is defined as the sum of contributions of all urban-related predictors with VIP values >1 , including UrbF, UrbV, and Δ UrbF (Section 3.2). Then, by dividing their individual contributions by CT_{urb} , the contributions of UrbF, UrbV, and Δ UrbF to the total urbanization influence of CoHot events are estimated. Similarly, the contribution of vegetation change is the sum of Δ LAI and Δ FVC.

3. Results

3.1. Urbanization and observed CoHot changes in China

Fig. 2a illustrates the linear trend of UrbF within the 1-km radius of the CMA stations, which can be interpreted as the rate of urbanization. Most stations located in eastern China (east of 110°E) experienced a significant increase in UrbF ($>8\%$ per decade) during 1971–2017, while stations in central and western China showed a slower rate of urbanization. In 2017, 1314 stations had an UrbF larger than 33% (defined as urban stations according to previous works) (Ma and Yuan, 2021; Wang et al., 2021), with 76% of these stations located east of 110°E. UrbH and UrbV display a distinct north-south aggregation pattern, with high and

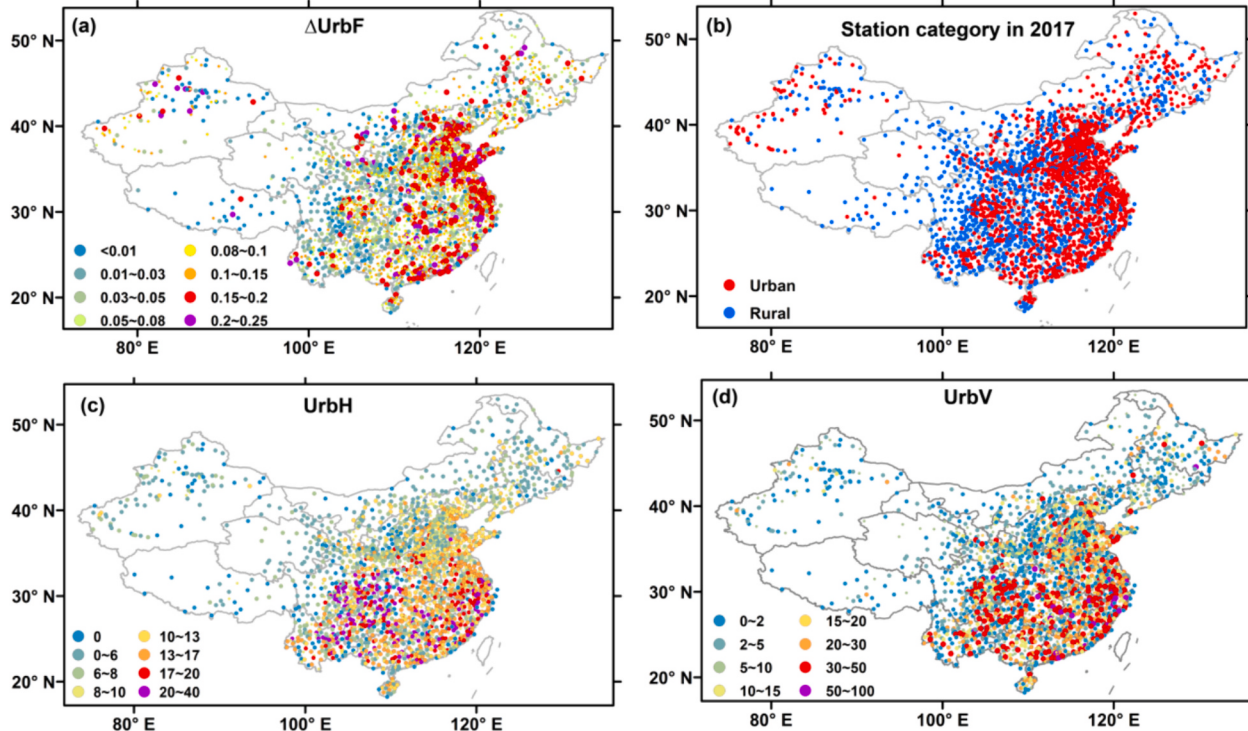


Fig. 2. Station locations and their urbanization characteristics. (a) Linear trend of urban fraction (UrbF; $-/decade$) during 1971–2017. (b) Urban and rural stations in 2017. (c) Urban building height (UrbH; m) and (d) building volume density (UrbV; m^3/km^2) over different stations. All values are averaged around the 1-km radius of the stations.

low values primarily appearing in southern (south of 35°N) and northern China, respectively. There is a significant ($p < 0.1$) spatial correlation between ΔUrbF and both UrbH (0.55) and UrbV (0.63), indicating that stations with rapid urbanization typically have higher building heights and volume densities.

Fig. 3a depicts the observed trend in CoHot frequency. Most stations show an increasing trend in CoHot frequency, consistent with findings based on the gridded HadGHCND dataset (Wang et al., 2020a). However, about 2% of stations exhibit a negative trend, predominantly located in northern and northeastern China, indicating strong spatial heterogeneity at the station scale. The trend exceeds 1 event/decade in eastern and southern coastal areas, some regions in central China (25–35°N, 110°–118°E), and eastern Sichuan Province (28–32°N, 104–106°E), more than double that of northern and northwestern China (**Fig. 3g-h**). After averaging the station values at the provincial scale, this north-south disparity becomes even more pronounced, with average trends of 0.2–0.6 events/decade in the southern regions and 0.05–0.2 events/decade in the northern regions (**Fig. 3b**). The changes in duration are similar to those in frequency (**Fig. 3d-e**), but the intensity trends show a larger positive magnitude (>1 °C/decade) in northern and northwestern China (**Fig. 3g-h**).

Clustering analysis reveals distinct aggregation patterns in CoHot

changes (**Fig. 3c, f and i**). The east China and the eastern part of Sichuan province are hotspots of the CoHot changes by showing significantly larger increasing trends of all the three characteristics than other regions. The south and north China, however, are hotspots of increasing CoHot frequency/duration and intensity, respectively. Such a spatial gathering pattern for CoHot long-term changes is different from that for CoHot characteristics, where the north China Plain (34°N to 41°N; 113°E to 121°E) and the south China are defined as the hotspot and coldspot of CoHot duration, respectively (Yang et al., 2022). Therefore, more attention should be given to the rising CoHot events in southern China.

3.2. Evaluation of the PLSR model and identification of dominant factors

Fig. 4a-f depict the evaluation results of the PLSR model. Overall, the simulated results align closely with the observed results, as they are distributed near the 1:1 line, with the average relative simulation errors of 23.4%, 32.3% and 11.4% at station scales for frequency, duration, and intensity, respectively (**Fig. 4a-c**). Based on independent evaluation (green dots in **Fig. 4a-c**), the PLSR model explains 61–74% of the total variance observed at the station scale. At the regional scale, the simulation accuracy of the PLSR model improves further, with average

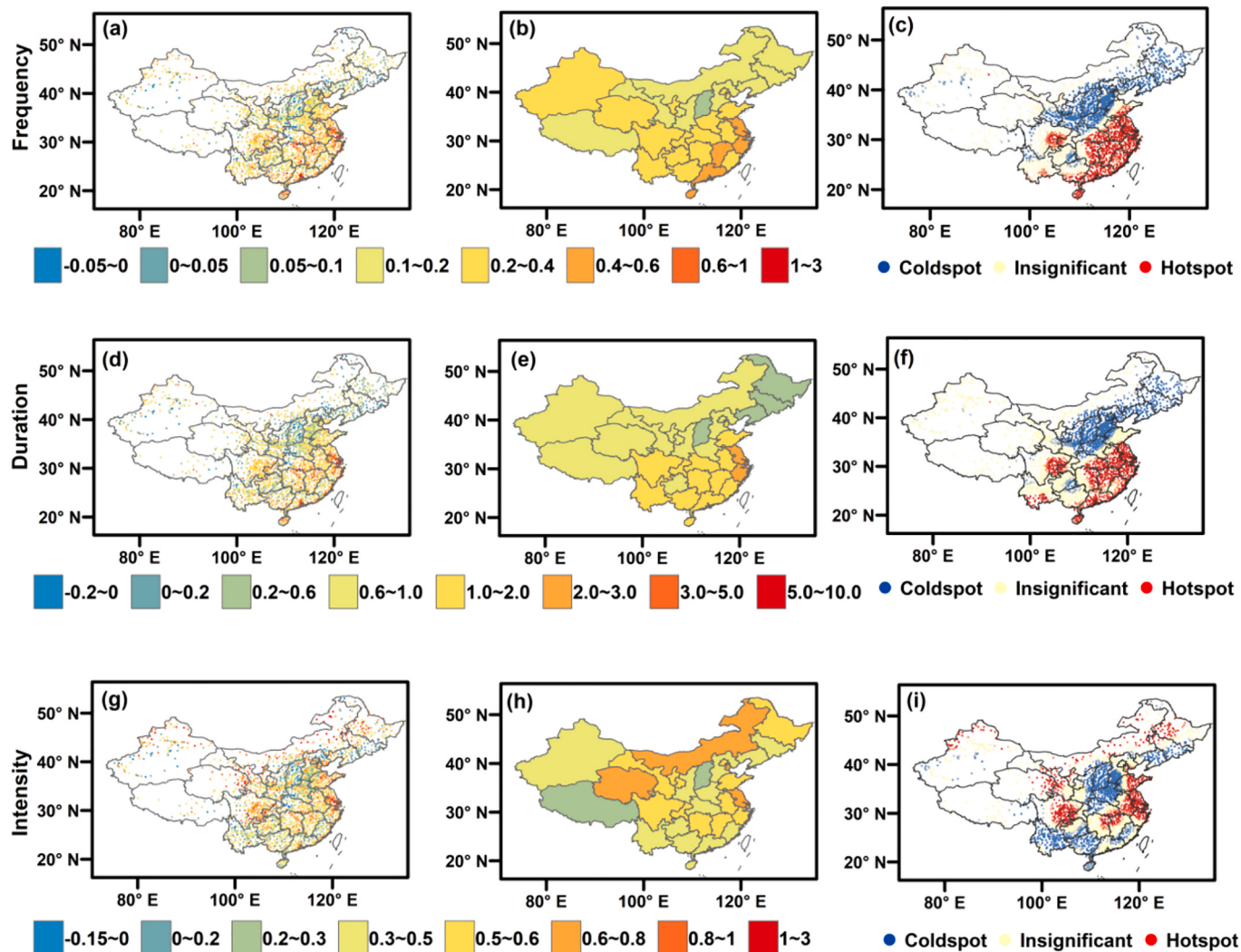


Fig. 3. Linear trends of different compound hot extremes (CoHot) characteristics during 1971–2017. (a) Linear trends of CoHot frequency (events/decade) during 1971–2017 at station scales. (b) The same as (a), but for the mean trends at provincial scales averaged from stations. (c) Hotspots and coldspots of the trend according to the Getis-ord Gi^* method, where hotspots (or coldspots) mean that the grid and its surrounding region tend to experience significantly ($p < 0.1$) larger (or smaller) trend than the average level. (d-f) and (g-i) are the same as (a-c), but for CoHot duration (days/decade) and severity ($^{\circ}\text{C}/\text{decade}$).

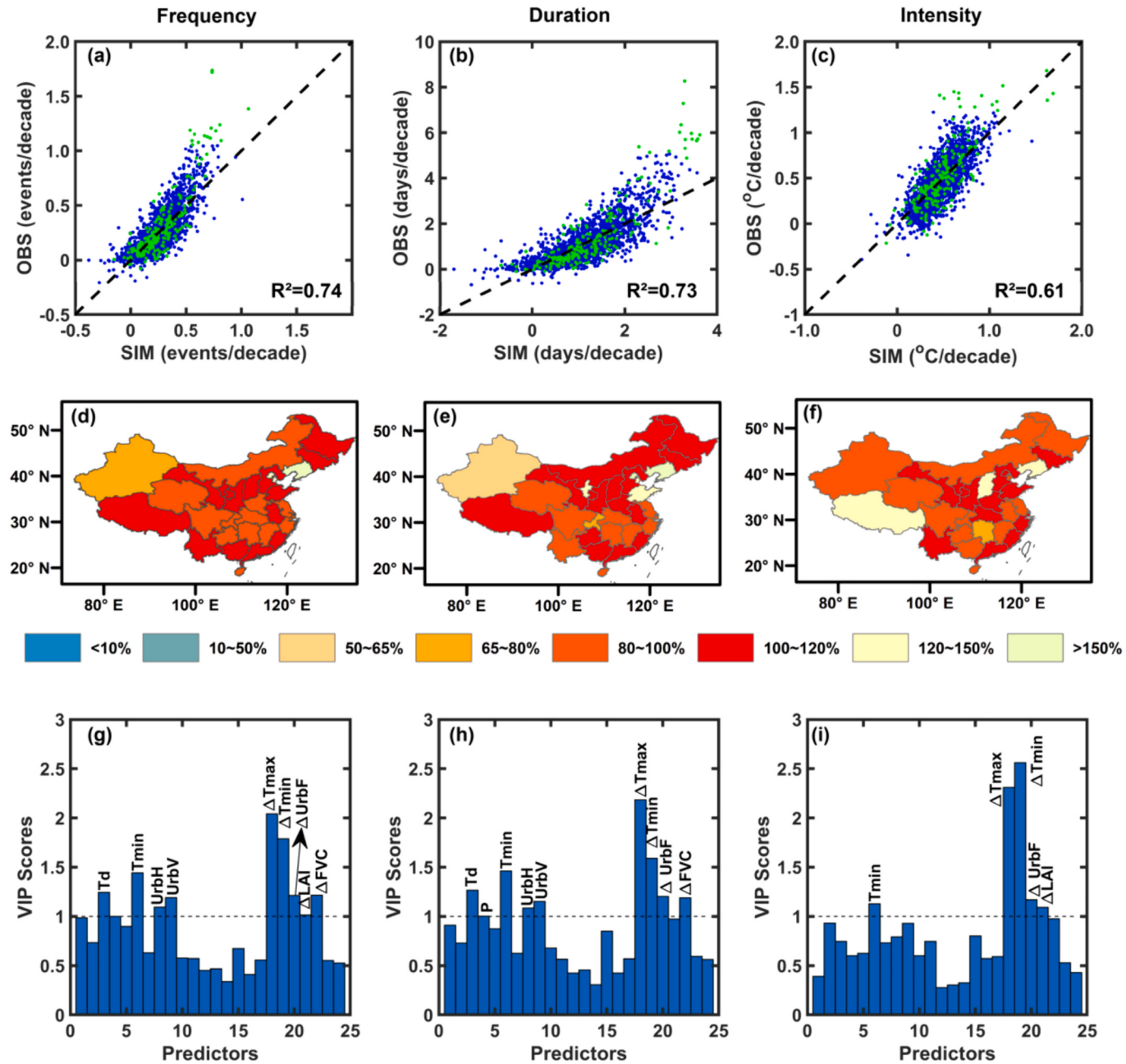


Fig. 4. Evaluation of the partial least squares regression (PLSR) model in simulating long-term trends of compound hot extremes (CoHot) characteristics at station and regional scales. (a-c) Scatter plot of the simulation and observation. Blue dots are samples used in model calibration, while green dots are independent samples used only in evaluation. (d-f) Percentage of the simulated trends against the observed ones at regional scales. Regional mean trends were first calculated from station values, and the ratio of simulated regional mean trends to the observed one was derived. (g-i) Variable importance for projection (VIP) scores of different predictors, with the predictors whose VIP score is larger than 1 shown directly. Left column: CoHot frequency; Medium column: CoHot duration; Right column: CoHot intensity. (For interpretation of the references to colour in this figure legend, the reader is referred to the web version of this article.)

relative simulation errors of 3.8%, 6.4%, and 2.6% for frequency, duration, and intensity, respectively (Fig. 4d-f). At the national scale, the average observed trends for CoHot frequency, duration, and intensity are 0.27 events/decade, 1.12 days/decade, and 0.47 $^{\circ}\text{C}/\text{decade}$, individually, while the corresponding simulated results are 0.26 events/decade, 1.11 days/decade, and 0.47 $^{\circ}\text{C}/\text{decade}$. Therefore, the PLSR model, using numerous environmental and urbanization-related predictors, performs well across scales from station to national level, with the relative modeling error changing from approximately 20% at the station scale to 4% at the national scale.

Fig. 4g-i show the VIP scores of different predictors in the PLSR model. Overall, the dominant predictors with VIP values >1 vary in

frequency, duration, and intensity, indicating the complex mechanisms or pathways of numerous factors in influencing CoHot changes. The long-term trends of summertime maximum and minimum temperatures (ΔT_{Max} and ΔT_{Min}) exhibit the highest VIP values for all three characteristics. This is reasonable as warmer summers can directly increase the probability of CoHot events occurring (Wang et al., 2020b). The climate background, including the T_d , T_{min} and P , is also important, especially for interpreting the spatial differences of CoHot frequency and duration changes. The regression coefficients of T_d , T_{min} and P (not shown) are positive, suggesting that the occurrence and duration of CoHot events are easier to increase over regions with a humid and warm climate background. This is consistent with the positive spatial

correlation between these three climate factors and changes in CoHot characteristics (Fig. S1).

Urban-related factors, including the UrbH, UrbV, and Δ UrbF are critical for changes in CoHot frequency and duration, but only Δ UrbF has a significant impact on changes in CoHot intensity (Fig. 4g-i). The VIP score of UrbV is much larger than that of UrbH, indicating that the urban building volume density is more important than building height. The regression coefficients of UrbV, and Δ UrbF are positive in the PLSR model, while the regression coefficient of UrbH is negative except for the CoHot intensity, indicating that the influence of UrbV/ Δ UrbF and UrbH is positive and negative, respectively. In addition, vegetation greening/wilting (indicated by Δ LAI and Δ FVC) are also shown to be important, with negative regression coefficients, indicating that vegetation greening has a mitigating effect on CoHot events. Physical interpretations for the positive/negative impacts of these factors are discussed in the Section 4.2.

Based on the VIP scores in Fig. 4, climate change factors (e.g., Δ Tmin and Δ Tmax) are more important than urbanization and vegetation changes. This result is consistent with previous work (Wang et al., 2021), which showed that the contribution of climate change induced by anthropogenic greenhouse gases emission is twice that of urbanization. However, the importance of these factors is time-variant and may change with climate change and urbanization processes (Wu et al., 2023a). Therefore, we calculated the VIP score within a 30-year moving window from 1985 to 2002 to investigate the dynamics of the dominant predictors' importance (Fig. 5). The VIP scores for climate background

(Td and P), urbanization-related factors (UrbH, UrbV, and Δ UrbF), and changes in vegetation cover (Δ FVC) increase significantly from <1 to >1 across all CoHot characteristics (except for the negative trend of Td and P in CoHot intensity), with urbanization-related factors generally exhibiting the largest increases. Note that the precipitation (P) is considered as an important factor, as its VIP value is >1 throughout the period (Fig. 4h) and in recent decades (e.g., 2000–2001 values in Fig. 5a and c). The VIP scores for Δ Tmin and Δ Tmax show a declining trend in CoHot frequency and duration. Therefore, compared to the temperature change (Δ Tmin and Δ Tmax), the relative importance of urbanization and vegetation greening on changes in CoHot frequency and duration has increased in recent years. Possible reasons might include the enhanced human activities (e.g., grain for green project) and accelerated urbanization in recent decades (Chen et al., 2013).

3.3. Contribution of different factors to CoHot changes

Fig. 6a shows the contributions of different dominant factors to the nationwide average changes in CoHot frequency. Note that urbanization predictors with VIP values larger than 1 (e.g., UrbH, UrbV, and Δ UrbF) are selected to represent the contribution of urbanization (dark green in Fig. 6a). Overall, the contributions of UrbH, UrbV, and Δ UrbF are -3.1%, 9.0% and 3.4%, respectively. Therefore, the total contribution of urbanization to the increased CoHot frequency is 9.3% (-3.1% + 9.0% + 3.4%). The contributions of Δ Tmax and Δ Tmin are 45.9% and 65.3%, respectively (yellow and orange bars in Fig. 6a). The contribution of

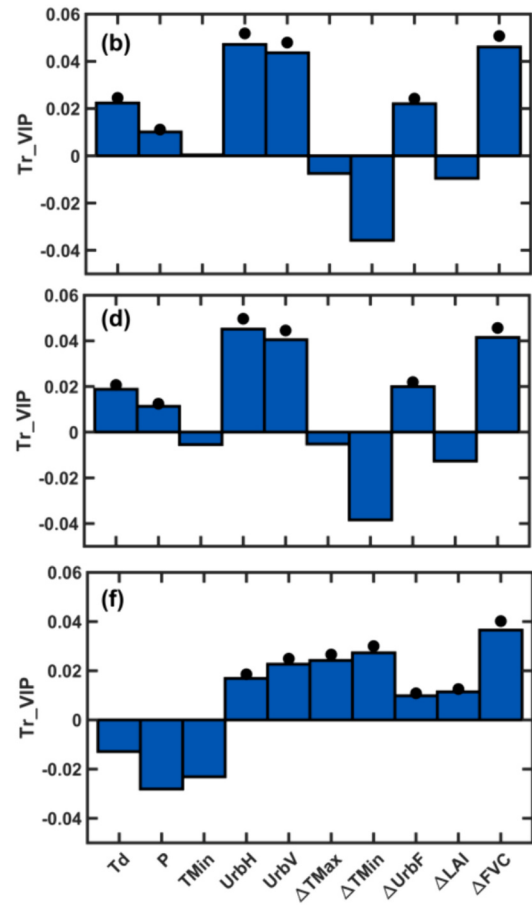
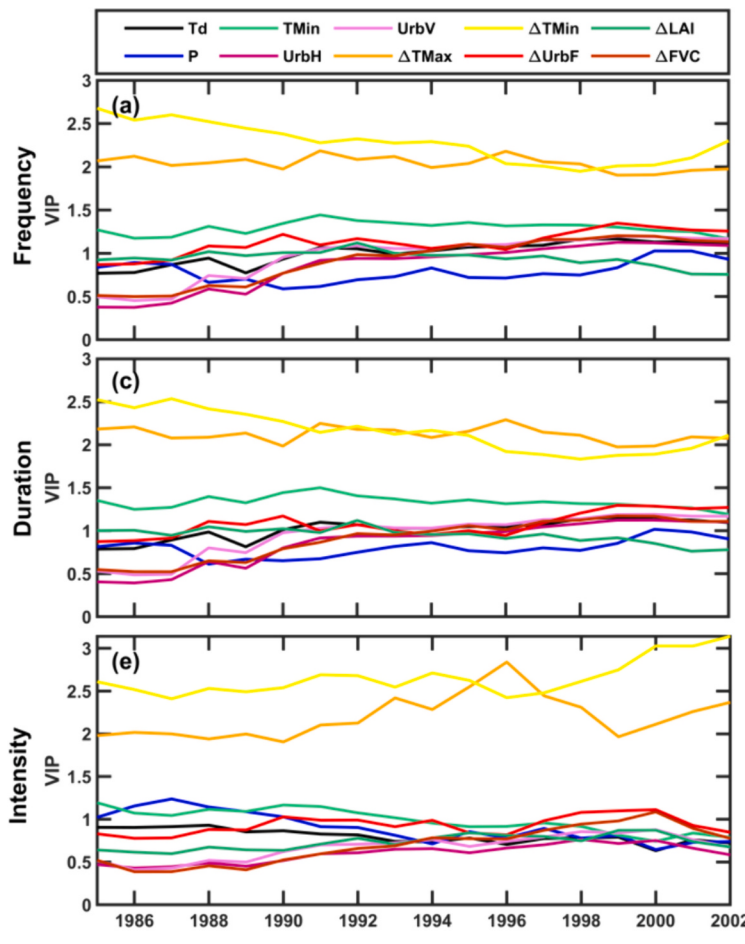


Fig. 5. Changes and linear trends of the Variable importance for projection (VIP) scores of the dominant controlling factors during 1985–2002. (a) Time series of VIP scores for different factors in estimating changes of compound hot extremes frequency during 1985–2002 with a 30-year smoothing window. (b) The linear trends of VIP scores in (a), with the black dots indicating significant trends. (c-d) and (e-f) are the same as (a-b), but for duration and severity.

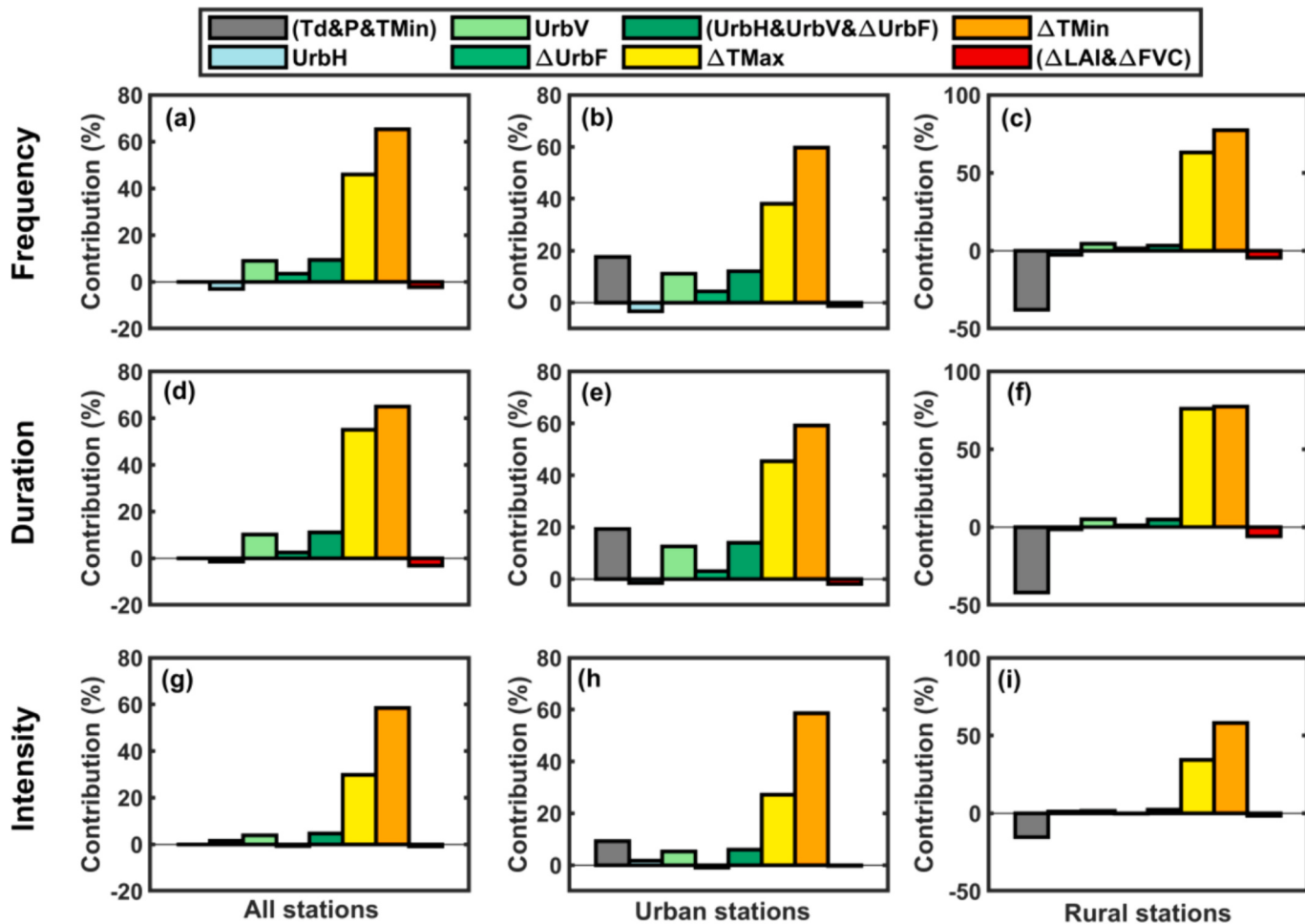


Fig. 6. Contributions of different factors to the trends of compound hot extremes (CoHot) characteristics at national scales. National mean CoHot trends were first calculated and then the contributions were derived. The left column means all stations were used, while the middle and right column mean only urban and rural stations were included, respectively. Factors include climatology of dew point temperature (Td), precipitation (P), summertime minimum temperature (TMin), urban building height (UrbH) and volume density (UrbV), and long-term trends of urban fraction (Δ UrbF), summertime minimum (Δ TMin) and maximum (Δ TMax) temperature, leaf area index (Δ LAI), and fraction of vegetation cover (Δ FVC).

climate background and vegetation change (Δ LAI and Δ FVC) are 0% and -2.3% , respectively, which are relatively smaller compared to urbanization- and climate change-related factors (gray and red bars in Fig. 6a). The results for duration are similar to those for frequency, with changes in average summertime temperature dominating the long-term trend and urbanization contributing 11.1% (Fig. 6d). However, the contribution of urbanization to changes in CoHot intensity is only 4.6%, which is only one third of its contribution to frequency and duration (Fig. 6g). Based on the urban fraction in 2017, stations were further grouped into urban and rural ones. For urban stations, the contribution of urbanization increases to 6–14% while the contributions of Δ TMax and Δ TMin decrease to 27–45% and 59–60%, respectively (Fig. 6b). Notably, the contribution of a warm and humid climate background increases sharply in urban stations, as most urban stations are located over southeastern China, where the temperature and precipitation are higher. For rural stations, they are mostly located over western and central China, and the contribution of climate background becomes negative, and the impact of urbanization is smaller.

Fig. 7 depicts the contributions of different factors to the regional average trends in CoHot frequency, duration, and intensity. The warming of average summertime temperatures (Δ Tmax and Δ Tmin) contributes $>100\%$ over northern China, while over southern China, the contribution is 40–60%. The total contributions of climate background, changes in other meteorological forcings and surface albedo are

negative (not shown), partially offsetting the substantial positive contribution of temperature changes. For example, an increase in surface albedo will dampen the increasing trend of CoHot events against the background of temperature warming. The contribution of urbanization to frequency and duration can reach up to 10–20%, primarily over southern China, the North China Plain, and northeastern China, while it is $<10\%$ in other regions (Fig. 7d–e). Consistent with the national-scale results in Fig. 6, the contribution of urbanization to intensity is only 1/3–1/2 of its contribution to frequency and duration (Fig. 7f). Moreover, when we focus on stations experiencing rapid urbanization, the contribution of urbanization to CoHot frequency and duration increases to 10–30%, and its contribution to CoHot intensity is 8–15%, mainly concentrated in southern China (Fig. S2). The contributions of LAI and vegetation cover changes generally range between $\pm 10\%$, with larger negative contributions observed over northern China, where significant vegetation greening (both in vegetation cover and LAI) has occurred in recent decades (Fig. 7g–i, Fig. S3).

We also calculated the contribution of urbanization and vegetation change at the regional scale within a 30-year moving window from 1985 to 2002. Urbanization's contribution generally increases from 1971 to 1999 (centered at 1985) to 1988–2017 (centered at 2002), especially for CoHot frequency and duration (Fig. S4). For the vegetation change, its negative and positive contributions increase significantly in northern China (e.g., Shaanxi, Gansu and Shanxi) and southern China (e.g.,

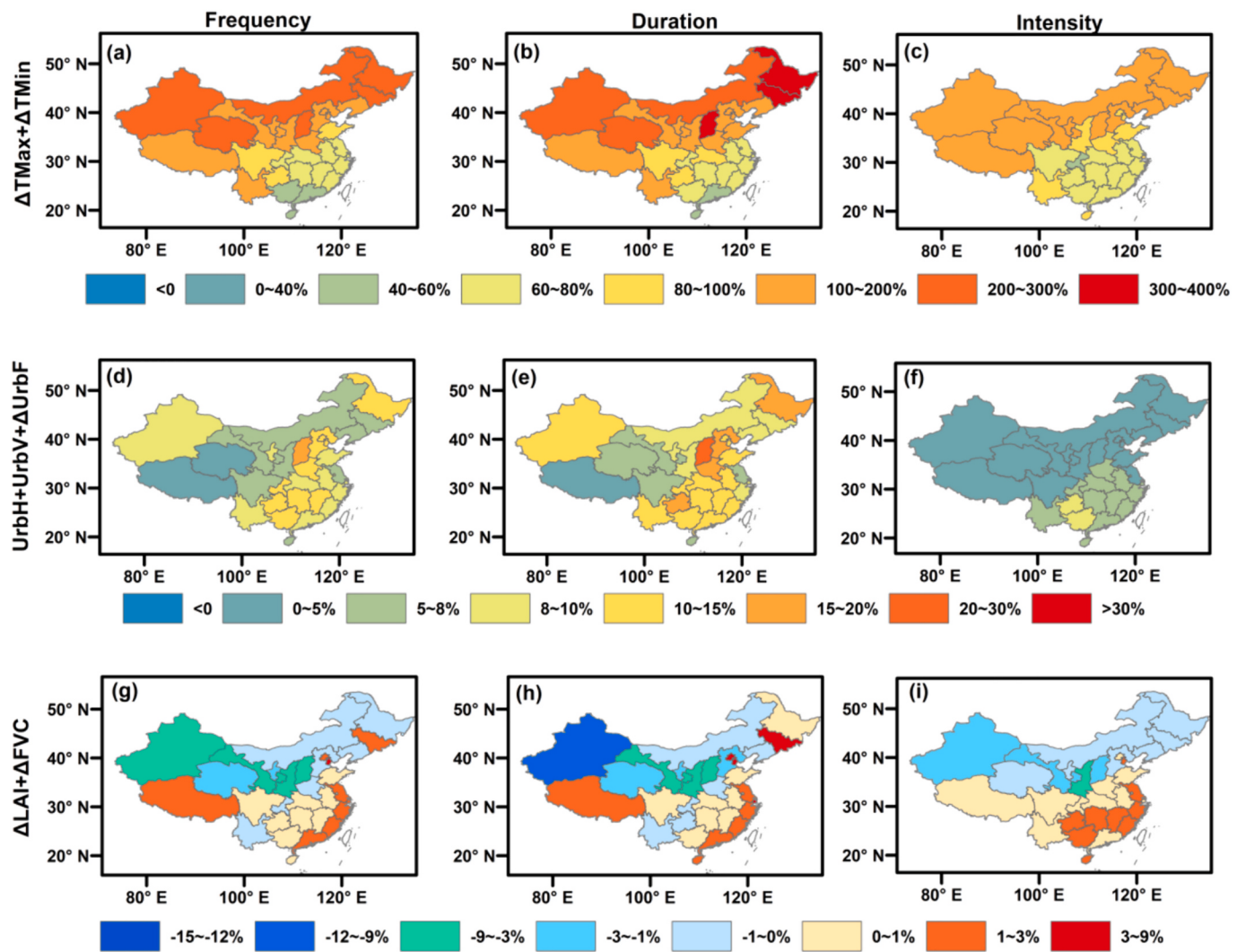


Fig. 7. Contribution of different factors to the changes of compound hot extremes (CoHot) at regional scales. Factors include urban building height (UrbH) and volume density (UrbV), and long-term trends of urban fraction (ΔUrbF), summertime minimum (ΔTMin) and maximum (ΔTMax) temperature, leaf area index (ΔLAI), and fraction of vegetation cover (ΔFVC).

Jiangsu, Zhejiang and Sichuan), respectively (Fig. S5). Therefore, consistent with the VIP score, the contribution of urbanization and vegetation change is increasing in recent decades.

Fig. 8 provides a comprehensive picture of the urbanization's effect on CoHot changes at the grid scales. Large positive contribution values (>40%) can be found in the city centers due to the fast urbanization speed and larger building volume densities. The subplots for three major metropolitan regions show that the contribution of urbanization decreases gradually from the city center to the surrounding rural regions, with contribution values ranging between 2% and 5% in most rural grids. Fig. 8 also indicates that, the impact of urbanization on CoHot frequency and duration is more than twice that on intensity over most regions except the central of Pearl River Delta. The total contribution of urbanization is further divided into building height (UrbH), building volume (UrbV), and impervious area changes (ΔUrbF) (not shown). The gridded mean contributions of UrbH, UrbV, and ΔUrbF to the total urbanization's effect on CoHot frequency (duration or intensity) are -14.2% (-11.8% or 30.7%), 68.5% (77.6% or 72.0%), and 45.7% (34.2% or -2.7%), respectively. Therefore, in addition to the commonly concerned changes in urban impervious surfaces, the 3-D urban structure, particularly the building volume density, is critical for increasing the CoHot frequency, duration, and intensity. Although such a result is based on the statistical analysis, it is consistent with the recent research

on urban heat island which simulated urban climates of various generated cities under the same climate background and suggested that the urban density is directly related to the strength of urban heat island (Li et al., 2020a).

Similarly, LAI and changes in vegetation cover have caused significant CoHot variations at the grid scale over northern China, where there has been extensive vegetation greening (Fig. 9a, d, g). The contribution of vegetation greening (including increases in LAI and FVC) to frequency/duration reaches -40% (Fig. 9b, e), while its contribution to intensity is -20% (Fig. 9b, e, h). It is worth noting that the significant contribution of $\Delta \text{LAI} + \Delta \text{FVC}$ to frequency and duration over southwestern China is due to the relatively smaller magnitude of CoHot changes there. In addition, the mitigation effect of vegetation greening over northern China is dominated by the vegetation cover change, as the contribution of ΔFVC is similar to the sum of $\Delta \text{LAI} + \Delta \text{FVC}$ (Fig. 9c, f and i). The strong mitigation effect occurs mainly over northern China is because both FVC and LAI show a strong increasing trend there (Fig. S3). However, only the LAI increases over southern China and the LAI is not an important factor for the changes of CoHot frequency and duration (Fig. 4), therefore the mitigation effect of vegetation greening on CoHot is limited over southern China. This analytical result is consistent with the previous modeling work, which also suggested that vegetation greening mainly cools the land surface over northern China (Yu et al.,

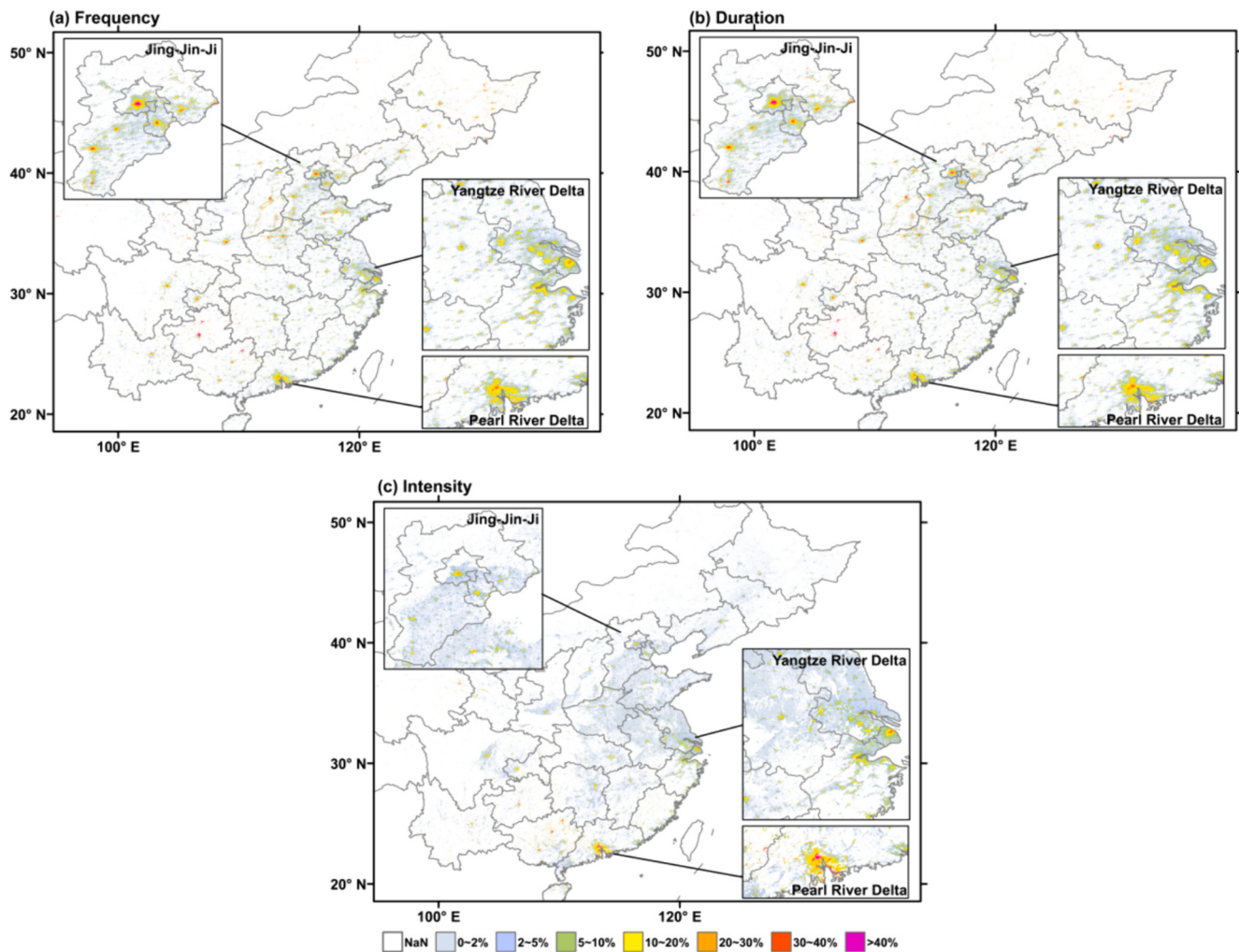


Fig. 8. Contribution of urbanization to the changes of compound hot extremes (CoHot) at 1 km resolution. The NaN indicates no buildings. Three large metropolitan regions, namely Jing-Jin-Ji, Yangtze River Delta, and Pearl River Delta, are depicted in subplots.

2020).

4. Discussion

4.1. Advantages and limitations of the PLSR-based method

Compared to the dynamic classification method that divides stations into urban and rural ones each year and compares the differences in CoHot changes, the PLSR-based method has the following advantages. 1) The PLSR-based framework supports multiscale analysis, while dynamic classification methods are typically applied to a large rectangular area (usually $5^\circ \times 5^\circ$) to cover urban and rural stations over the entire period. 2) The PLSR-based framework can quantify the influences of different urbanization factors. For example, our results not only show that urbanization can increase the frequency, duration and intensity of CoHot, but also indicate that this positive impact is mainly attributed to the high building volume density and the increasing impervious areas in urban regions. 3) The PLSR-based framework provides a comprehensive overview of the contributions of various environmental factors to CoHot changes, making it easy to compare the relative importance of numerous processes (e.g., climate background, climate change, urbanization and vegetation change).

However, the PLSR-based framework also has some limitations. Firstly, if the nonlinearity in the data is very strong, it may not be possible for PLSR model to accurately capture and characterize the

relationship. For example, urbanization and vegetation change can influence precipitation and temperature downstream through atmospheric circulations (Lang et al., 2023; Xing et al., 2019), but these non-local effects on CoHot changes cannot be captured by the PLSR-based framework. Conducting land-atmosphere coupled simulations with convective permitting scales, including urban canopy and dynamic vegetation modules, can be used to quantify the indirect effects of urbanization and vegetation change (Guo et al., 2019, 2020). However, conducting decadal long simulations with convective permitting scales over continents incurs extremely high computational costs. Secondly, the PLSR model is calibrated using station data across China, inevitably leading to the loss of some regional features and resulting in relatively large simulation errors in some regions (e.g., the Tibet region). Future research could establish different PLSR models for different regions, but this approach will be constrained by the issue of sparse observation stations in some regions (e.g., the Tibet region). Although there are some uncertainties, the results of this work remain reliable considering the high simulation accuracy of the PLSR model in most regions and the roles of different factors in modulating CoHot changes revealed by PLSR model are physically interpretable (Section 4.2).

4.2. The different roles of factors in CoHot changes

The attribution results indicate that Td, P, Tmin, UrbH, UrbV, ΔUrbF, ΔTmax, ΔTmin, ΔLAI and ΔFVC are the dominant factors influencing

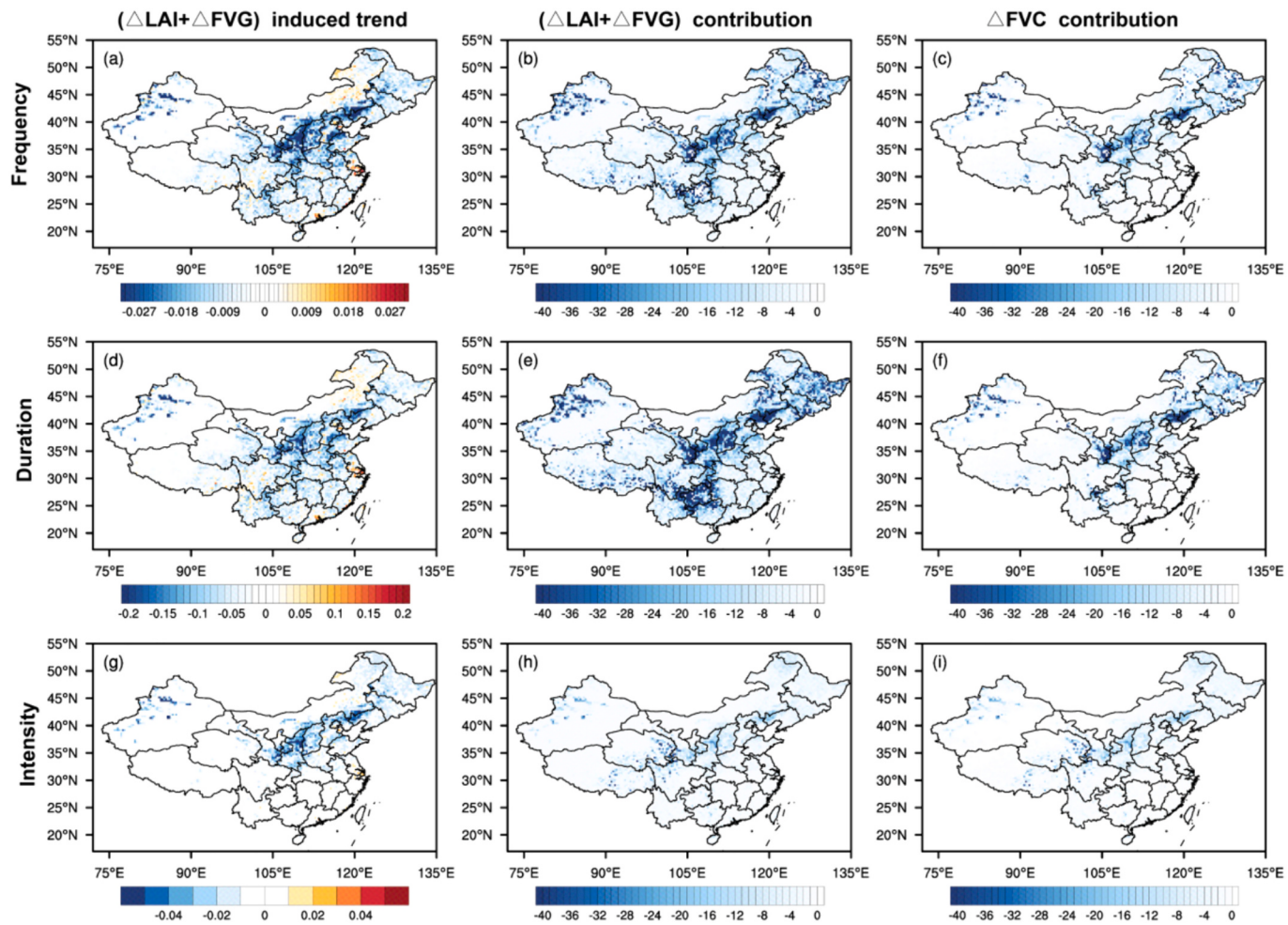


Fig. 9. Total effects of LAI change (ΔLAI) and vegetation cover fraction change (ΔFVC) on compound hot extremes (CoHot) changes at 1 km resolution. (a) Trend of CoHot frequency (events/decade) induced by ΔLAI and ΔFVC . (b) Contributions of ΔLAI and ΔFVC to the simulated frequency changes. (c) Contributions of ΔFVC to the simulated frequency changes. (d-f) and (g-i) are the same as (a-c), but for duration (days/decade) and intensity ($^{\circ}\text{C}/\text{decade}$) changes.

CoHot changes. Td, P, Tmin, UrbV, ΔUrbF , ΔTmax and ΔTmin exhibit positive effects, while UrbH, ΔLAI and ΔFVC show negative effects. The negative and positive effects of climate background, climate change, urbanization and vegetation processes on CoHot changes revealed by the PLSR model are consistent with previous studies and are physically interpretable.

A warm and humid climate can significantly reduce convective efficiency, resulting in local warming in urban areas (Manoli et al., 2019; Zhao et al., 2014), which promotes the development of heat waves. A higher building volume density typically has a larger heat capacity and higher anthropogenic heat fluxes, which helps to increase and sustain the urban canopy temperatures (Liu et al., 2021), thus having a positive impact on CoHot changes. The positive effect of ΔUrbF may be related to the smaller surface heat capacity and reduced evapotranspiration cooling intensity caused by the increase in impervious areas (Li et al., 2019). However, taller buildings increase surface roughness and enhance heat exchange between the urban canopy and the upper atmosphere (Li et al., 2019). Moreover, taller buildings enhance shading effect and reduce heat storage in street canyons during daytime (Li et al., 2020b). These two processes can mitigate the frequency and duration of heat extremes in urban areas. The mitigation effects of increased LAI and vegetation cover can be explained through the following processes: 1) increasing evapotranspiration and reducing surface temperatures (Wu et al., 2024); 2) increasing surface albedo (especially in urban areas) and reducing incoming solar radiation (Wong et al., 2021); 3) increasing summertime precipitation in China and reducing hot risks (Yu et al., 2020). While the

influence of various factors on CoHot changes can be interpreted based on the above approaches, modeling work is needed in the future to provide in-depth analysis of these physical mechanisms.

5. Conclusion

This study systematically attributes the long-term changes in characteristics of summertime CoHot in China to various factors (e.g., climate background, urbanization, vegetation and climate change) using Partial Least Square Regression (PLSR) and Variable Importance Projection (VIP). Notably, the contributions of different urbanization factors (e.g., impervious area changes, building height and building volume density) to the overall effects of urbanization are separated, which is critical for formulating sustainable urban development policies. The main conclusions are summarized as follows:

- (1) Over the past 50 years, the frequency, duration, and intensity of summertime CoHot in China have increased at rates of 0.27 events/decade, 1.12 days/decade, and $0.47^{\circ}\text{C}/\text{decade}$, respectively. The CoHot change trends exhibit a distinct north-south heterogeneity pattern, with southern and northern China being hotspots for changes in frequency/duration and intensity, respectively. The PLSR-based model successfully simulates the long-term trends of CoHot characteristics, with the relative modeling error changing from approximately 20% at the station scale to 4% at the national scale.

- (2) The hot and humid climate background, warming of summertime mean maximum and minimum temperatures, expansion of urban impervious areas, higher building volume density, and vegetation wilting are main factors favoring the increasing trend in CoHot frequency, duration and intensity. Although the changes in summertime mean maximum and minimum temperatures are the most important for CoHot changes, the importance of other dominant factors has gradually increased in recent years, particularly the influence of urbanization.
- (3) Urbanization's contribution to the trend of CoHot characteristics has escalated from 9.3% at the national scale to over 40% at the grid (1-km) scale, with its contribution to the frequency/duration being approximately twice that of intensity trends. Extensive vegetation greening in northern China, including increased LAI and expanded vegetation cover, can mitigate locally increased CoHot frequency/duration by 40%. In addition, the positive impact of urbanization is mainly driven by high building volume density (68.5–77.6%), followed by the expansion of impervious area (−2.7–45.7%), and building height (−11.8–30.7%). Conversely, mitigation influence of vegetation greening is primarily attributed to increased vegetation cover rather than LAI.

CRediT authorship contribution statement

Peng Ji: Conceptualization, Methodology, Writing – original draft, Validation, Methodology. **Xing Yuan:** Conceptualization, Methodology, Writing – review & editing. **Feng Ma:** Resources, Methodology. **Qibo Xu:** Writing – review & editing.

Declaration of competing interest

The authors declare that they have no known competing financial interests or personal relationships that could have appeared to influence the work reported in this paper.

Data availability

The station observations of TMax and TMin is from China Meteorological Data Service Center hold by CMA (<http://data.cma.cn/en>). The ERA5 data is available at Copernicus Climate Data Store (<https://cds.climate.copernicus.eu/>). GAIA data set can be downloaded from the Star Cloud Data Service Platform (<https://data-starcloudpcl.ac.cn/>), while 3-D building structure data is available at <https://www.landbigdata.info/cscproject/dataset.html>. GLASS products are from <http://www.glass.umd.edu/>, while TerraClimate dataset is available from <https://www.climatologylab.org/terraclimate.html>.

Acknowledgments

This work was supported by Natural Science Foundation of Jiangsu Province (BK20220460), National Natural Science Foundation of China (42305175), and the Major Science and Technology Program of the Ministry of Water Resources of China (SKS-2022019).

Appendix A. Supplementary data

Supplementary data to this article can be found online at <https://doi.org/10.1016/j.atmosres.2024.107632>.

References

- Abatzoglou, J.T., Dobrowski, S.Z., Parks, S.A., Hegewisch, K.C., 2018. Data Descriptor: TerraClimate, a high-resolution global dataset of monthly climate and climatic water balance from 1958–2015. *Sci. Data* 5.
- Carlson, T.N., Boland, F.E., 1978. Analysis of Urban-Rural Canopy using a surface heat flux/temperature model. *J. Appl. Meteorol.* 17 (7), 998–1013.
- Chao, L.Y., Huang, B.Y., Yuanjian, Y., Jones, P., Cheng, J.Y., Yang, Y., Li, Q.X., 2020. A new evaluation of the role of urbanization to warming at various spatial scales: evidence from the Guangdong-Hong Kong-Macau Region, China. *Geophys. Res. Lett.* 47.
- Chen, Y., Zhai, P.M., 2017. Revisiting summertime hot extremes in China during 1961–2015: Overlooked compound extremes and significant changes. *Geophys. Res. Lett.* 44, 5096–5103.
- Chen, M.X., Liu, W.D., Tao, X.L., 2013. Evolution and assessment on China's urbanization 1960–2010: under-urbanization or over-urbanization? *Habitat Int.* 38, 25–33.
- Easterling, D.R., Evans, J., Groisman, P.Y., Karl, T., 2000. Observed variability and trends in extreme climate events: a brief review. *Bull. Am. Meteorol. Soc.* 81, 417–425.
- Farrés, M., Platikanov, S., Tsakovski, S., Tauler, R., 2015. Comparison of the variable importance in projection (VIP) and of the selectivity ratio (SR) methods for variable selection and interpretation. *J. Chemom.* 29, 528–536.
- Getis, A., Ord, J.K., 1992. The analysis of spatial association by use of distance statistics. *Geogr. Anal.* 24, 189–206.
- Gong, P., Li, X.C., Wang, J., Bai, Y.Q., Cheng, B., Hu, T.Y., Liu, X.P., Xu, B., Yang, J., Zhang, W., Zhou, Y.Y., 2020. Annual maps of global artificial impervious area (GAIA) between 1985 and 2018. *Remote Sens. Environ.* 236.
- Grimmond, S., 2007. Urbanization and global environmental change: local effects of urban warming. *Geogr. J.* 173, 83–88.
- Guo, Z.Y., Fang, J., Sun, X.G., Yang, Y., Tang, J.P., 2019. Sensitivity of summer precipitation simulation to microphysics parameterization over Eastern China: convection-permitting regional climate simulation. *J. Geophys. Res.-Atmos.* 124, 9183–9204.
- Guo, Z.Y., Fang, J., Sun, X.G., Tang, J., Yang, Y., Tang, J.P., 2020. Decadal long convection-permitting regional climate simulations over eastern China: evaluation of diurnal cycle of precipitation. *Clim. Dyn.* 54, 1329–1349.
- Hair, J.F., Sarstedt, M., Ringle, C.M., 2019. Rethinking some of the rethinking of partial least squares. *Eur. J. Mark.* 53, 566–584.
- Hersbach, H., Bell, B., Berrisford, P., Hirahara, S., Horányi, A., Muñoz-Sabater, J., Nicolas, J., Peubey, C., Radu, R., Schepers, D., Simmons, A., Soci, C., Abdalla, S., Abellán, X., Balsamo, G., Bechtold, P., Biavati, G., Bidlot, J., Bonavita, M., Chiara, G., Dahlgren, P., Dee, D., Diamantakis, M., Dragani, R., Flemming, J., Forbes, R., Fuertes, M., Geer, A., Haimberger, L., Healy, S., Hogan, R.J., Hólm, E., Janisková, M., Keeley, S., Laloyaux, P., Lopez, P., Lupu, C., Radnoti, G., Rosnay, P., Rozum, I., Vamborg, F., Villaume, S., Thépaut, J.N., 2020. The ERA5 global reanalysis. *Q. Roy. Meteorol. Soc.* 146, 1999–2049.
- Iang, X., Zhang, D.L., Luo, Y.L., 2023. Influences of Urbanization on an Afternoon Heavy Rainfall Event over the Yangtze River Delta Region. *Mon. Weather Rev.* 151, 815–832.
- IPCC, 2021. Summary for policymakers. In: *Climate Change 2021: The Physical Science Basis. Contribution of Working Group I to the Sixth Assessment Report of the Intergovernmental Panel on Climate Change*. Cambridge University Press, Cambridge, pp. 1–3949.
- Karl, T.R., Knight, R.W., 1997. The 1995 Chicago heat wave: how likely is a recurrence? *Bull. Am. Meteorol. Soc.* 78, 1107–1119.
- Li, D., Liao, W.L., Rigden, A.J., Liu, X.P., Wang, D.G., Malyshev, S., Sheviakova, E., 2019. Urban heat island: Aerodynamics or imperviousness? *Sci. Adv.* 5.
- Li, M.M., Koks, E., Taubenböck, H., van Vliet, J., 2020a. Continental-scale mapping and analysis of 3D building structure. *Remote Sens. Environ.* 245.
- Li, Y.F., Schubert, S., Kropp, J.P., Rybski, D., 2020b. On the influence of density and morphology on the Urban Heat Island intensity. *Nat. Commun.* 11 (1).
- Li, Z.X., Hu, J.X., Meng, R.L., He, G.H., Xu, X.J., Liu, T., Zeng, W.L., Li, X., Xiao, J.P., Huang, C.R., Du, Y.D., Ma, W.J., 2021. The association of compound hot extreme with mortality risk and vulnerability assessment at fine-spatial scale. *Environ. Res.* 198.
- Li, W.L., Sun, B., Wang, H.J., Zhou, B.T., Li, H.X., Xue, R.F., Duan, M.K., Luo, X.C., Ai, W.W., 2023. Anthropogenic impact on the severity of compound extreme high temperature and drought/rain events in China. *NPJ Clim. Atmos. Sci.* 6.
- Liang, S.L., Cheng, J., Jia, K., Jiang, B., Liu, Q., Xiao, Z.Q., Yao, Y.J., Yuan, W.P., Zhang, X.T., Zhao, X., Zhou, J., 2021. The Global Land Surface Satellite (GLASS) product suite. *B. Am. Meteorol. Soc.* 102, E323–E337.
- Liao, W.L., Li, D., Malyshev, S., Sheviakova, E., Zhang, H.H., Liu, X.P., 2021. Amplified increases of compound hot extremes over Urban Land in China. *Geophys. Res. Lett.* 48.
- Lin, X., Wang, Y., Song, L., 2024. Urbanization amplified compound hot extremes over the three major urban agglomerations in China. *Geophys. Res. Lett.* 51, e2023GL106644.
- Liu, X., Yue, W.Z., Zhou, Y.Y., Liu, Y., Xiong, C.S., Li, Q., 2021. Estimating multi-temporal anthropogenic heat flux based on the top-down method and temporal downscaling methods in Beijing, China. *Resour. Conserv. Recycl.* 172.
- Ma, F., Yuan, X., 2021. More persistent summer compound hot extremes caused by global urbanization. *Geophys. Res. Lett.* 48.
- Mahieu, B., Qannari, E., Jaillais, B., 2023. Extension and Significance Testing of Variable Importance in Projection (VIP) indices in Partial Least Squares regression and Principal Components Analysis. *Chemometr. Intell. Lab.*, p. 242.
- Manoli, G., Fatichi, S., Schläpfer, M., Yu, K.L., Crowther, T.W., Meili, N., Burlando, P., Katul, G.G., Bou-Zeid, E., 2019. Magnitude of urban heat islands largely explained by climate and population. *Nature* 573, 55–60.
- Meehl, G.A., Tebaldi, C., 2004. More intense, more frequent, and longer lasting heat waves in the 21st century. *Science* 305, 994–997.
- Paschalidis, A., Chakraborty, T.C., Fatichi, S., Meili, N., Manoli, G., 2021. Urban forests as main regulator of the evaporative cooling effect in cities. *AGU Adv.* 2.

- Shao, L.D., Liao, W.L., Li, P.L., Luo, M., Xiong, X.H., Liu, X.P., 2023. Drivers of global surface urban heat islands: Surface property, climate background, and 2D/3D urban morphologies. *Build. Environ.* 242.
- Sobstyl, J.M., Emig, T., Qomi, M.J.A., Ulm, F.J., Pelleng, R.J.M., 2018. Role of city texture in urban heat Islands at Nighttime. *Phys. Rev. Lett.* 120.
- Taha, H., 1997. Urban climates and heat islands: Albedo, evapotranspiration, and anthropogenic Heat. *Energ. Build.* 25, 99–103.
- Wang, L., Li, D., 2021. Urban heat islands during heat waves: a comparative study between Boston and Phoenix. *J. Appl. Meteorol. Climatol.* 60, 621–641.
- Wang, J., Chen, Y., Tett, S.F.B., Yan, Z.W., Zhai, P.M., Feng, J.M., Xia, J.J., 2020a. Anthropogenically-driven increases in the risks of summertime compound hot extremes. *Nat. Commun.* 11.
- Wang, J., Feng, J.M., Yan, Z.W., Chen, Y., 2020b. Future risks of unprecedented compound heat waves over three vast urban agglomerations in China. *Earths Future* 8.
- Wang, J., Chen, Y., Liao, W.L., He, G.H., Tett, S.F.B., Yan, Z.W., Zhai, P.M., Feng, J.M., Ma, W.J., Huang, C.R., Hu, Y.M., 2021. Anthropogenic emissions and urbanization increase risk of compound hot extremes in cities. *Nat. Clim. Chang.* 11, 1084–1089.
- Wang, X.X., Lang, X.M., Jiang, D., 2022. Detectable anthropogenic influence on summer compound hot events over China from 1965 to 2014. *Environ. Res. Lett.* 17.
- Wold, S., Johansson, E., Cochi, M., 1993. PLS: Partial Least Squares Projections to Latent Structures. ESCOM Science Publishers, Leiden.
- Wong, N.H., Tan, C.L., Kolokotsa, D.D., Takebayashi, H., 2021. Greenery as a mitigation and adaptation strategy to urban heat. *Nat. Rev. Earth Env.* 2, 166–181.
- Wu, G.A., Lu, X.C., Zhao, W., Cao, R.C., Xie, W.Q., Wang, L.Y., Wang, Q.H., Song, J.X., Gao, S.B., Li, S.G., Hu, Z.M., 2023a. The increasing contribution of greening to the terrestrial evapotranspiration in China. *Ecol. Model.* 477.
- Wu, S.J., Luo, M., Zhao, R., Li, J., Sun, P., Liu, Z., Wang, X.Y., Wang, P., Zhang, H., 2023b. Local mechanisms for global daytime, nighttime, and compound heatwaves. *NPJ Clim. Atmos. Sci.* 6.
- Wu, J., Feng, Y., Li, L.Z.X., Ciais, P., Piao, S.L., Chen, A.P., Zeng, Z.Z., 2024. Earth greening mitigates hot temperature extremes despite the effect being damped by rising CO₂. *One Earth* 7.
- Xie, W.X., Zhou, B.T., Han, Z.Y., Xu, Y., 2022. Substantial increase in daytime-nighttime compound heat waves and associated population exposure in China projected by the CMIP6 multimodel ensemble. *Environ. Res. Lett.* 17.
- Xing, Y., Ni, G.H., Yang, L., Yang, Y., Xing, P., Sun, T., 2019. Modeling the impacts of urbanization and open water surface on heavy convective rainfall: a case study over the emerging Xiong'an City, China. *J. Geophys. Res.-Atmos.* 124, 9078–9098.
- Xu, Q., Chen, W., Song, L., 2022. Two leading modes in the evolution of major sudden stratospheric warmings and their distinctive surface influence. *Geophys. Res. Lett.* 41, e2021GL095431.
- Yang, Y., Zhao, N., Wang, Y.W., Chen, M.X., 2022. Variations in summertime compound heat extremes and their connections to urbanization in China during 1980–2020. *Environ. Res. Lett.* 17.
- Yu, L.X., Liu, Y., Liu, T.X., Yan, F.Q., 2020. Impact of recent vegetation greening on temperature and precipitation over China. *Agric. For. Meteorol.* 295.
- Yu, Y.F., You, Q.L., Zuo, Z.Y., Zhang, Y.Q., Cai, Z.Y., Li, W., Jiang, Z.H., Ullah, S., Tang, X., Zhang, R.H., Chen, D.L., Zhai, P.M., Shrestha, S., 2023. Compound climate extremes in China: trends, causes, and projections. *Atmos. Res.* 286.
- Zhang, X.B., Hegerl, G., Zwiers, F.W., Kenyon, J., 2005. Avoiding inhomogeneity in percentile-based indices of temperature extremes. *J. Clim.* 18, 1641–1651.
- Zhao, L., Lee, X., Smith, R.B., Oleson, K., 2014. Strong contributions of local background climate to urban heat islands. *Nature* 511, 216–219.
- Zhao, J.C., Meili, N., Zhao, X., Fatichi, S., 2023. Urban vegetation cooling potential during heatwaves depends on background climate. *Environ. Res. Lett.* 18.